



University of Warwick institutional repository: <http://go.warwick.ac.uk/wrap>

This paper is made available online in accordance with publisher policies. Please scroll down to view the document itself. Please refer to the repository record for this item and our policy information available from the repository home page for further information.

To see the final version of this paper please visit the publisher's website. Access to the published version may require a subscription.

Author(s): M.J. Knight, F. Allegretti, 1, E.A. Kröger, K.A. Hogan, D.I. Sayago, T.J. Lertholli, W. Unterberger and D.P. Woodruff

Article Title: The local structure of SO₂ and SO₃ on Ni(1 1 1): A scanned-energy mode photoelectron diffraction study

Year of publication: 2009

Link to published version: <http://dx.doi.org/10.1016/j.susc.2009.04.001>

Publisher statement: None

The local structure of SO₂ and SO₃ on Ni(111): a scanned-energy mode photoelectron diffraction study

M. J. Knight¹, F. Allegretti¹⁺, E. A. Kröger², K. A. Hogan³, D. I. Sayago², T. J. Lerotholi¹,
W. Unterberger², D. P. Woodruff^{1♦},

¹ *Physics Dept, University of Warwick, Coventry CV4 7AL, UK*

² *Fritz-Haber-Institut der Max-Planck-Gesellschaft, Faradayweg 4-6, 14195 Berlin, Germany*

³ *Dept. of Chemical & Biological Sciences, University of Huddersfield, Queensgate, Huddersfield HD1 3DH, UK*

Abstract

O 1s and S 2p scanned-energy mode photoelectron diffraction (PhD) data, combined with multiple-scattering simulations, have been used to determine the local adsorption geometry of the SO₂ and SO₃ species on a Ni(111) surface. For SO₂, the application of reasonable constraints on the molecular conformation used in the simulations leads to the conclusion that the molecule is centred over hollow sites on the surface, with the molecular plane essentially parallel to the surface, and with both S and O atoms offset from atop sites by almost the same distance of 0.65 Å. For SO₃, the results are consistent with earlier work which concluded that surface bonding is through the O atoms, with the S atom higher above the surface and the molecular symmetry axis almost perpendicular to the surface. Based on the O 1s PhD data alone, three local adsorption geometries are comparably acceptable, but only one of these is consistent with the results of an earlier normal-incidence X-ray standing wave (NIXSW) study. This optimised structural model differs somewhat from that originally proposed in the NIXSW investigation.

Keywords: photoelectron diffraction; chemisorption; surface structure; nickel; sulphur dioxide; sulphite; low index single crystal surfaces

⁺ Now at Institute of Physics, Surface and Interface Physics, Karl-Franzens University Graz, A-8010 Graz, Austria

[♦] corresponding author: email d.p.woodruff@warwick.ac.uk

1. Introduction

SO₂ is an atmospheric pollutant, and the main source of 'acid rain', arising from the burning of fossil fuels, so its catalytic chemistry is of considerable practical importance. As a result, there have been quite a number of model surface science studies of its interaction with metal surfaces. At low temperatures, the molecule adsorbs intact on many surfaces, but some form of reaction typically occurs below room temperature to produce surface SO_x species, with disproportionation to coadsorbed atomic S and SO₃ being reported on many surfaces, including those of Ni. Reaction of SO₂ with surface atomic oxygen on these surfaces also leads to enhanced SO₃ production. Experimental quantitative structural investigations of both SO₂ and SO₃ have been performed on a small number of surfaces, including several on the low-index faces of Ni (on (100) [1, 2], on (110) [3, 4] and on (111) [1, 5, 6]). On all of these Ni surfaces S K-edge NEXAFS (near-edge X-ray absorption fine structure) measurements have indicated that SO₂ adsorbs with its molecular plane essentially parallel to the surface, while on Ni(111) the same technique has led to the conclusion that SO₃, produced by disproportionation, is adsorbed on the surface with its internal C_{3v} symmetry axis essentially perpendicular to the surface [6].

The local adsorption site in these adsorption systems is, however, less clear. In the case of the Ni(111) surface, the subject of the present study, two rather different adsorption geometries have been proposed for the intact SO₂ species. Using SEXAFS (surface extended X-ray absorption fine structure), Yokoyama *et al.* [1] favour a geometry in which the S atom occupies a bridge site, whereas Jackson *et al.* [5, 6] conclude that their NIXSW (normal incidence X-ray standing wavefield) measurements are consistent with the molecule being centred over a hollow site. The hollow site geometry was also found to give the best quantitative fit in multiple-scattering simulations [7] of the experimental NEXAFS data published by Yokoyama *et al.* and reproduced by Jackson *et al.* A B3LYP density functional theory (DFT) cluster calculation [8] of this adsorption structure, in which the substrate being modelled by just 4 Ni atoms, was found to favour the bridge site model of Yokoyama *et al.* More recently, however, a DFT slab calculation (using the

CASTEP code) [9] concluded that the optimised bridge and hollow geometries (fig. 1) are energetically the most favoured structures, but the difference in calculated adsorption energies was too small to provide a reliable basis for identifying the preferred geometry. However, these same calculations also found that the structural parameter values (the exact lateral position of the molecule on the surface) for the bridge geometry did not agree with those of the experimental SEXAFS investigation. In particular, while the SEXAFS experiments concluded that the S atom lies (exactly) in a bridging site, the DFT calculations yield an optimised bridging geometry for the molecule in which the S atom is displaced significantly towards an atop site (fig.1). Indeed, a DFT structural optimisation performed with the SEXAFS-derived structure as the starting model actually converged on the hollow site geometry. Of the two structural models proposed on the basis of experimental studies, these DFT results thus appear to favour the hollow adsorption site for SO₂ on Ni(111). However, new experimental data, from an entirely different structural technique, may provide a more definitive means of resolving this controversy.

With this objective in mind, we present here the results of an investigation of this adsorption system using scanned-energy mode photoelectron diffraction (PhD). Our investigation also includes a similar study of the local structure of the SO₃ species on Ni(111). Only one experimental determination of this structure has so far been published, by Jackson *et al*, based on NIXSW measurements [6]. The favoured adsorption geometry for this species corresponds to surface bonding through oxygen atoms, with the S atom (higher above the surface) in a bridging site relative to the outermost Ni substrate layer (fig. 1). DFT calculations [9] yield a closely-similar optimal structure. Here we present the results of the experimental PhD investigation of these two adsorption systems, and also consider how these results may be reconciled with the detailed findings of the earlier experimental and theoretical investigations. We find further supporting evidence for the occupation of the hollow site by adsorbed SO₂; for SO₃ the optimal lateral positioning of the molecule on the surface differs from the conclusions of the earlier NIXSW study, but we show that the new geometry is, in fact, consistent with the NIXSW experimental data.

2. Experimental Details and Surface Characterisation

The experiments were conducted in a conventional ultra-high vacuum surface science end-station equipped with the usual facilities for sample cleaning, heating and cooling. This instrument was installed on the UE56/2-PGM-1 beamline of BESSY II which comprises a 56 mm period undulator followed by a plane grating monochromator [10]. Different electron emission directions can be detected by rotating the sample about its surface normal (to change the azimuthal angle) and about a vertical axis (to change the polar angle). Sample characterisation *in situ* was achieved by LEED and by soft-X-ray photoelectron spectroscopy (SXPS) using the incident synchrotron radiation. These wide-scan SXPS spectra, and the narrow-scan O 1s and S 2p spectra used in the PhD measurements, were obtained using an Omicron EA-125HR 125 mm mean radius hemispherical electrostatic analyser, equipped with seven-channeltron parallel detection, which was mounted at a fixed angle of 60° to the incident X-radiation in the same horizontal plane as that of the polarisation vector of the radiation.

The Ni(111) crystal was cleaned *in situ* by several cycles of Ar ion bombardment followed by brief annealing to 800 K. This was followed by 2-3 cycles of *in situ* chemical cleaning to remove residual surface carbon, achieved by annealing the sample in 1×10^{-8} mbar of oxygen for 2 min, followed by brief heating to 700 K in ultra-high vacuum. The resulting surface was clean and well-ordered as indicated by SXPS of the S 2p, C 1s and O 1s spectral regions and by a (1x1) LEED pattern. Prior to initial dosing with SO₂ the chamber walls were conditioned by several 30 minute exposures to a partial pressure of SO₂ of 5×10^{-8} mbar; this ensured that subsequent introductions of SO₂ to the chamber did not lead to a strong reaction with the chamber walls and to the release of other more weakly bound species into the vacuum.

Fig. 2 shows the XP spectra in the kinetic energy range corresponding to the S 2p and O 1s peaks following exposure of the sample to SO₂ at low temperature (and after subsequent heating), recorded at nominal photon energies of 500 eV and 650 eV,

respectively. S 2p spectra comprise spin-orbit split doublets with a separation of approximately 1.2 eV, corresponding to each of the chemically-distinct S states on the surface, with a nominal intensity ratio of 1:2 for the 2p_{1/2} and 2p_{3/2} peaks, the latter having the higher kinetic energy. As we are primarily interested in *relative* photoelectron binding energies and chemical shifts, no calibration was undertaken of the binding energy scale, so all data are presented in terms of photoelectron kinetic energies. Evidently the spectra show three main chemically-shifted states, with 2p_{3/2} kinetic energies of approximately 332.8 eV, 334.6 eV, and 337.6 eV. The dominant peak following the lower SO₂ exposure is that at 334.6 eV and may be attributed to intact molecular SO₂ on the surface. The remaining two components, which become dominant after heating the surface to 210 K, are attributable to SO₃ (332.8 eV) and atomic S (337.6 eV), which arise as a consequence of the disproportionation reaction (e.g. $2 \text{SO}_2 \rightarrow \text{SO}_3 + \text{S} + \text{O}$, although other schemes with different final products are possible). These core-level shifts, and the progression of the surface reaction, are consistent with the results of earlier S 2p and S 1s photoemission investigations of SO₂ on Ni(110) [4], and Ni(111), [6] respectively. Evidently, the lower (0.8×10^{-6} mbar.s) exposure leads to a surface on which SO₂ is the dominant species, but some components of the reaction products are already present at low temperature. Heating to 210 K almost completely removes the SO₂ surface component. We note, though, that the near 1:1 ratio of the two peaks at kinetic energies consistent with the two spin-orbit split S 2p components from atomic S, together with the shoulder at ~335.5 eV kinetic energy, indicates that there may be a fourth S component present on the surface with a S 2p_{3/2} kinetic energy of approximately 336.5 eV. One possibility is that this is attributable to a different atomic S species, perhaps in a local sulphide.

The O 1s XP spectra of fig. 2 are consistent with this picture but provide relatively little additional information. There seems to be a small chemical shift of ~0.2 eV in the O 1s emission from the SO₂ and SO₃ species, while a shoulder at higher kinetic energy is probably attributable to atomic O. More troublesome is a lower kinetic energy feature (~115 eV) with a binding energy some 2 eV greater than that of SO₂ and SO₃. In an earlier S 2p photoemission study of SO₂ reaction with Ni(110) Wilde *et al.* [4] observed a

peak at this energy and attributed it to an unknown SO_x species which is transformed at higher temperatures. In the absence of any matching distinct S 2p peaks, however, and our observation that this peak grew very significantly over a period of hours when the sample was held at the lowest temperatures, we attribute this feature to molecular water contamination. The presence of this peak may be a consequence of the need to use a very long gas pipeline for the SO_2 to meet safety requirements at BESSY, but its effect could be minimised by the application of a number of precautions. Specifically, when performing the PhD experiments on the surface SO_2 species, holding the sample at a slightly elevated temperature of 145 K markedly reduced the accumulation of water from the residual vacuum. Moreover, when investigating the SO_3 species, the sample could be held at a higher temperature of ~ 160 K, further reducing this problem. No evidence was found for any influence of the presence of coadsorbed water, at different surface concentrations, on the S 2p XPS data.

One further experimental detail of note concerns the influence of the incident monochromated synchrotron radiation on the molecular adsorbate layer. The experimental results reported here were recorded in three separate allocations of synchrotron radiation beamtime over a period of 14 months. The last of these, conducted to provide further verification of some of the data collected earlier, was performed after some significant modifications had been made to the post-monochromator focussing to produce a much-reduced beam size. Using this beam, very significant radiation-induced effects, mainly of photon-stimulated desorption of SO_2 , but also some enhanced surface reaction, were observed, on a timescale significantly shorter than that required for collection of PhD modulation spectra (~ 1 -2 hours). Clearly this is a consequence of the much-increased photon flux density at the sample due to the ‘improved’ beamline optics. Fortunately, attenuation of the beam with a polyimide foil allowed new data to be collected that did not suffer from either the severe contamination of the earlier experiments nor this problem of radiation damage. Despite these problems, comparisons of PhD data taken in the two runs in the same experimental geometry did indicate an overall consistency in the measured modulation spectra.

The PhD technique [11, 12] exploits the coherent interference of the directly emitted

component of the photoelectron wavefield from a core level of an adsorbate atom with components of the same wavefield elastically scattered by the surrounding atoms, and particularly backscattered from the substrate atoms. As the photon energy, and thus the photoelectron energy and associated photoelectron wavelength, are changed, these scattering paths switch in and out of phase. This leads to intensity modulations which can be analysed, with the aid of multiple-scattering simulations, to establish the local structural environment of the emitter atoms. In the present case, measurements were made of photoelectron diffraction from both the S 2p and O 1s emission, providing a potential means of determining the local sites of the S and O atoms in a largely independent fashion. These measurements were achieved by recording a sequence of photoelectron energy distribution curves (EDCs) around the S 2p and O 1s peaks at equal steps in photon energy in the photoelectron kinetic energy range of ~ 60 -370 eV, for each of a number of different emission directions in the polar emission angle range from 0° (normal emission) to 40° , in the $[\bar{1}10]$, $[\bar{1}2\bar{1}]$ and $[\bar{2}11]$ azimuths (see fig. 3 for the definition of these azimuths). These data were processed following our general PhD methodology (e.g. [11, 12]) in which the individual EDCs are fitted by the sum of Gaussian peaks, a step and a template background. The O 1s EDCs from the SO₂ as-prepared surfaces were fitted to three components (water, SO₂ and atomic O), while for the SO₃ preparation only two components (SO₃ and atomic O) proved necessary. The S 2p EDCs were fitted by spin-orbit split pairs of peaks with the peak width of the 2p_{1/2} component constrained to be equal to that of the 2p_{3/2} peak. The integrated areas of the adsorbate-derived peaks (with the 2p_{1/2} and 2p_{3/2} peaks summed for the S 2p data) were then plotted as a function of photoelectron energy and each final PhD modulation spectrum was obtained by subtraction of, and normalisation by, a smooth spline function representing the non-diffractive intensity and instrumental factors. For the SO₂ data, the sets of spectra were checked carefully to ensure that only those data with no evidence of beam-induced damage and minimal contamination by water were used in the final PhD analysis. The effect of carbon contamination in the beamline optics, leading to a strong C absorption edge in the incident radiation, persistently led to a 'glitch' in the S 2p PhD modulation spectra at a kinetic energy of around 120 eV, so only the data points above 130 eV were used in the structural analysis.

PhD data were collected from the surface SO_2 species on a surface prepared by using the lower exposure of 0.8×10^{-6} mbar.s, while data from the SO_3 species was collected from a surface first pre-exposed to 0.2×10^{-6} mbar.s of molecular oxygen, followed by the SO_2 exposure (2.0×10^{-6} mbar.s at ~ 100 K) and progressive heating to 210 K to achieve the optimal conversion of SO_2 to SO_3 as judged by the S 2p spectra. The reaction with the chemisorbed atomic oxygen led to a significantly higher coverage of SO_3 and less coadsorbed SO_2 .

3. PhD Results and Structure Analysis

3.1 SO_2

A full quantitative structure determination using PhD requires, as in quantitative LEED, the use of multiple-scattering simulations for a series of trial model structures. In some cases, however, some indication of the associated structure can be obtained by less thorough evaluation. In particular, a characteristic feature of PhD spectra is that strong backscattering modulations, with a single dominant (long) period, commonly occur in emission directions in which there is a substrate atom directly behind the emitter; in such cases it is this near-neighbour backscattering which tends to dominate the modulation spectra. In the present case none of the measured PhD modulation spectra (seven O 1s and eight S 2p PhD spectra in different emission directions that matched the required quality criteria were extracted from the measurements) showed strong modulations. However, for both emitter atoms the strongest modulations (albeit only $\sim \pm 20\%$), with an apparent dominance of a single long-range periodicity in electron wave vector, occur at normal emission. This tends to suggest that both the S and O atoms may occupy off-atop sites. Exact atop sites would give strong long-period modulations at normal emission; displacing the emitters a few tenths of an Ångström unit from an atop site generally leads to an attenuation of the modulation amplitude, but retains the long period modulations at normal emission. In truth, this conclusion could be consistent with either of the previously-favoured local bonding geometries (fig. 1). Moreover, the fact there is clear and consistent evidence that the SO_2 molecular plane lies approximately parallel to the

surface, and that neither the S-O nor the O-O intramolecular distances match the Ni-Ni distances of the substrate, means that it is impossible for both O atoms to occupy high-symmetry substrate sites, and highly unlikely that the S atom also occupies such a site.

To pursue this more quantitatively, multiple-scattering simulations of a subset of the experimental PhD modulation spectra were performed; this subset comprised four spectra each from the S 2p and O 1s emitters, chosen to show the strongest modulations in a range of emission directions. These multiple-scattering spherical wave simulations are conducted on a large cluster of neighbouring scattering atoms. The computer code is based on a magnetic quantum number expansion and incorporates the effects of both finite energy and finite angular resolution which help to ensure rapid convergence [13, 14]. The initial unscattered photoelectron wavefield takes explicit account of the orbital character of the initial state, with the O 1s state giving rise to a *p*-wave and the S 2p state emitting into both *s* and *d*-waves whose relative amplitude and phase are accounted for. The optimisation procedure involves iteration of structural and vibrational parameters until the optimum theory-experiment agreement is reached, as measured objectively by a reliability factor (*R*-factor). The *R*-factor is defined [15] as the mean-square-difference between the theoretical and experimental modulation amplitudes, normalised such that a value of 0 corresponds to perfect agreement, 1 to no correlation, and 2 to anti-correlation. The precision of the results is determined by a variance which is defined in a similar fashion to that developed by Pendry for LEED [16]; this is described in detail in reference [17].

Initial calculations (using a reduced dataset of just two PhD spectra from each of the S 2p and O 1s emitters) were conducted for a range of variations of the two proposed adsorption geometries, bridge and hollow. Specifically, starting from a bridging position, the molecule was displaced laterally in the $\langle 110 \rangle$ azimuth, and starting from a hollow site, the displacement was in the $\langle 211 \rangle$ azimuth; these azimuthal directions are indicated by arrows in fig. 1 and correspond to mirror symmetry lines of the molecule and the outermost Ni surface layer. These lateral displacements were varied over the full range of periodicity of the substrate, and for each offset value variations of the height of the S and

O emitter sites above the surface were tested. For the purposes of these initial space-scanning calculations, the intramolecular conformation was constrained to be that of gas-phase SO₂ [18]. On fcc(111) surfaces there are actually two inequivalent three-fold coordinated hollow sites, referred to as the fcc and hcp hollows, located directly atop third-layer and second-layer substrate atoms, respectively. For a flat-lying molecule on such a surface one expects minimal difference in the energy of these two sites, so our calculations assumed these two hollow sites to be occupied with equal probability, and the same lateral offset (i.e. in identical geometries relative to the outermost Ni atom layer), although slight differences in the height of the molecule above the two hollows were allowed. The results identified two clear deep minima in the *R*-factor values, one for each of the two basic models. In both of these structures a common feature was that the S atom was laterally displaced from a Ni atop site by ~ 0.6 Å.

Further optimisation of these two models was then performed by simulating the full set of eight experimental PhD spectra, adjusting the exact positions of the O and S atoms on the surface, and also the vibrational amplitudes of the emitter and scatterer atoms, allowing anisotropy in the emitter vibrations, and also allowing the nearest-neighbour Ni atoms to take lower vibrational amplitudes than those of the Ni atoms in the bulk (as a means of accounting for correlated vibrations). These structural optimisations were performed in an automated fashion with the help of an adapted Newton-Gauss algorithm, using typically ~ 1200 single-scattering, ~ 800 double-scattering and ~ 400 triple scattering pathways. For the set of parameter values found for the best-fit structures, additional simulations were performed using a larger and more fully-converged set of scattering pathways; as in previous studies, this led to very small increases in the *R*-factor values, but confirmed the good quality of the experiment/theory comparisons for these structures. This two-stage process was adopted to keep computation times down to manageable levels and ensured a wide range of parameter space could be explored. For the hollow-site model, free optimisation of the structural models led to values of the S-O bondlength and the O-S-O bond angle of 1.50 Å and 111°, respectively (Table 1). The equivalent gas-phase values for molecular SO₂ are 1.43 Å and 118°, respectively, while the experimental SEXAFS study of SO₂ on Ni(111) provided a rather direct measurement of

the S-O bondlength of 1.48 ± 0.03 Å, this lengthening being consistent with the influence of the chemisorption. It is also notable that all the DFT calculations for SO₂ on Ni(111) (Table 2) indicate a significant reduction of the O-S-O bond angle relative to the gas-phase value. We therefore conclude that the freely-optimised conformation of SO₂ in the hollow-site model is reasonable. For the bridge-site model, on the other hand, this type of free optimisation led to values of these two parameters of 1.76 Å and 124.4°, respectively, the bondlength, at least, being unreasonably large. Additional calculations for the bridge-site model were therefore performed in which either the S-O bondlength or the O-S-O bond angle were constrained to values closer to the expected values. As seen in Table 1, constraining one of these parameters either led to an optimised value of the unconstrained parameter that was even further from the expected molecular conformation, or led to a very large increase in the *R*-factor value.

The origin of this apparent dilemma can be clearly traced to the fact that PhD is a highly local structural probe, and that the S 2p and O 1s PhD spectra are primarily sensitive to the location of the S and O atoms relative to the strongly-scattering Ni substrate atoms, and not to the relative positions of the S and O atoms which influence the data only through relatively weak intramolecular scattering. This is illustrated rather clearly by Fig. 4, which shows a *R*-factor contour map of the location of the two equivalent O atoms in the bridging geometry model with the S atom fixed at its optimum position for this model 0.58 Å off atop along the $\langle 110 \rangle$ symmetry line. When the O atom gets very close to the S atom intramolecular scattering does have a significant influence on the *R*-factor, but otherwise the contour lines are essentially circles centred on the next-neighbour Ni atoms, with the contours of minimum *R*-factor corresponding to the O atoms being ~ 0.65 Å off atop in any direction. The constraint that the S and O atoms are part of a SO₂ molecule, on the other hand, clearly means that most positions on these optimal contour lines are completely incompatible with any plausible molecular geometry. Superimposed on the contour map of fig. 4 are the specific constrained and unconstrained solutions. Clearly, acceptable fits to the S 2p and O 1s PhD data are not compatible with reasonable constraints on the S-O bondlength and O-S-O bond angle, whereas constraining these

parameters, that define the molecular conformation, to reasonable values, leads to poor fits to the PhD data.

By contrast, this difficulty does not arise when the molecule is more nearly centred on the hollow-site. In this case the unconstrained fits to the PhD data lead to an entirely reasonable molecular conformation. We therefore conclude that the PhD data, when combined with reasonable physical constraints on the solution, clearly distinguish these two models, and are only compatible with a hollow-site adsorption geometry. Fig. 5 shows a comparison of the experimental PhD spectra and the results of the multiple-scattering simulations for this best-fit hollow-site geometry. The associated structural parameter values are listed in Table 2 where they are compared with previously-determined values from other experimental and theoretical studies. These comparisons are discussed in section 4.

3.2 SO₃

Unlike the case of SO₂, for which the PhD spectra obtained from the O 1s and S 2p emitters showed modulations of comparable amplitude, the S 2p PhD spectra from the SO₃ species showed extremely weak modulations, of little more than $\pm 10\%$, with a peak-to-peak noise level of about half this amplitude. These spectra do not, therefore, provide a meaningful basis for a PhD structure determination of the S atom site in this molecular species. The O 1s PhD data, on the other hand, yielded modulation spectra with significantly better signal-to-noise ratio and somewhat larger modulations. This behaviour can be reconciled with the adsorption geometry previously favoured for SO₃ on Ni(111), and on some Cu surfaces, in which the O atoms bond to the surface and the S atoms lie several tenths of an Ångström unit higher above the Ni surface. This would lead to significantly larger S-Ni nearest-neighbour distances, and thus weaker PhD modulations from the strongly-scattering Ni surface atoms. This qualitative feature of the data thus provides some support for this adsorption geometry.

Our more quantitative structure determination is thus based entirely on O 1s PhD spectra

recorded from the SO₃-covered surface. While most possible adsorption sites on the surface lead to at least two structurally-distinct local O adsorption sites, it proved helpful to first identify which single O 1s emitter site provides the best fit to the PhD spectra. For this purpose, space-scanning calculations with a reduced number of scattering pathways were performed for a wide range of possible sites involving different lateral positions and heights above the surface, using a subset of PhD spectra measured in four different experimental geometries, two at normal emission (in different incidence azimuths), and one each at 10° and 20°. These calculations showed distinct *R*-factor minima with O-Ni interlayer spacings of ~1.9 Å in sites offset from atop towards the hollow sites by ~0.7Å.

More realistic space-scanning calculations were then performed on models that included the three distinct O emitters within a SO₃ species. In order to limit the number of such calculations, a number of constraints were applied. Firstly it was assumed, consistent with earlier findings, that the symmetry axis of the molecules lies approximately perpendicular to the surface. Second, it was assumed that at least some symmetry element of the free molecule (C_{3v}) and the substrate is shared. This led to two specific models ('hollow rotation 1' and 'hollow rotation 2' of fig. 6) in which a mirror plane of the substrate coincides with a mirror plane of the molecule, but each of these models allows all possible lateral positions within displacements parallel to the surface in a <211> azimuth along a line including atop and hollow-site geometries. In both of these models, two O atoms are in locally-equivalent sites, but the local site of the third O atom is different, except for the special cases of the exact atop and hollow sites where the C_{3v} symmetry axes of the molecule and the substrate coincide. The two models differ only in a 180° azimuthal rotation of the molecule. A third model considered, shown in the lower part of fig. 6 (labelled 'bridge'), involves displacement along a <110> line including atop and bridging sites; in this case, we have assumed that a mirror plane of the molecule coincides with a mirror plane of the outermost Ni layer, although this is *not* a mirror plane of the complete substrate. Notice that in this model the two O atoms that are mirror images of one another in this partial mirror plane are not formally equivalent (one O moving close to a fcc hollow while the other is similarly placed relative to a hcp hollow). Consistent with the application of this 'pseudo-mirror plane', the heights of these two O

atoms above the surface were constrained to be the same. Finally, a fourth model was considered in which the occupation of sites in the first two models, similarly located relative to fcc and hcp sites, was assumed to be equally probable. In these constrained molecular space-scanning calculations, the initial SO₃ geometry was assumed to be similar to that found in the earlier NIXSW and DFT studies, but the relative heights of the structurally-distinct O atoms and the S atom, as well as the lateral position, were adjusted to locate the local *R*-factor minima.

These calculations identified a total of 13 structures corresponding to such minima, with *R*-factor values in the range 0.17 to 0.47. Rejecting those structures with *R*-factors larger than the minimum value by more than the variance (0.04) reduced this number to 9. Inspection of the associated structural parameter values, however, revealed that several of these structures were closely similar. Firstly, it was clear that the *R*-factors and local structural parameters for individual structures in equivalent sites relative to fcc hollows, hcp hollows, and the combination of these two sites, were essentially identical. Further optimisation of this class of structures was thus only pursued on the mixed fcc + hcp model. The initially-optimised solutions then were found to all fit into one of three types. These were (see fig. 7): 'a': S atom in an off-hollow site with all three O atoms in off-atop sites; 'b': S atom in an off-bridge site such that one O atom is off-atop and the other two O atoms are located between hollow and bridging sites; 'c': S atom in an off-hollow site with all three O atoms in off-hollow sites. Further structural optimisation was therefore performed on one structure of each of these types. In selecting the structures to be considered in further detail, it was noted that while the overall *R*-factor calculated for the four different experimental geometries fell in the range 0.17-0.21, the individual *R*-factor for one PhD spectrum recorded in one particular geometry (20° polar emission angle) showed a particularly large variation (from 0.24 to 0.65), so the structures with the lowest values for this geometry were selected.

This further refinement of the structural models was performed with a larger set of experimental PhD spectra (six rather than four, including spectra recorded at 20° polar angle in all three measurement azimuths), using a larger number of scattering pathways in

the calculations to achieve acceptable convergence, and allowing re-adjustment of all the main structural parameters and optimisation of the vibrational amplitudes, including anisotropy in the vibrations of the emitter O atoms and the effect of nearest-neighbour correlations in the vibrations. The resulting overall R -factor values for the three structures were: 'a': 0.23, 'b': 0.22, 'c': 0.25. The variance of 0.04 (unchanged from the earlier results due to the opposing effects of the increased data set and the higher minimum value) does not allow us to formally reject any of these structural solutions on the basis of these PhD results alone. These three structures are shown schematically in fig. 7, while the associated structural parameter values are listed in Table 3. Examples of the quality of the agreement between theory and experiment for structures 'a' and 'b' are shown in fig. 8.

4. Discussion

4.1 SO₂

Previous experimental investigations of the local adsorption geometry of SO₂ on Ni(111) have led to two conflicting conclusions. Based on S K-edge SEXAFS Yokoyama *et al.* [1] concluded that the S atom occupies a bridging site on the surface, and thus proposed that the molecule (shown to have its molecular plane essentially parallel to the surface by NEXAFS) adopts an overall (off-) bridging geometry, somewhat similar to that shown in Fig. 1. By contrast, later NIXSW measurements [6] led to the conclusion that both the S and O atoms of the molecule occupied local off-atop sites, a result that could only be reconciled with hollow-site occupation of the molecule as a whole, also shown in fig. 1. Subsequently, a full theoretical investigation based on DFT calculations [9] that explored both of these (and other) adsorption geometries came to the interesting conclusion that two different local structures, with the molecule in hollow and bridging sites, exactly as shown in fig. 1, had almost the same total energy. Although this calculation thus appears not to resolve the controversy, it is important to note that the bridging structure found in the DFT study differs significantly from that proposed in the SEXAFS study; in particular, the S atom in the DFT structure is significantly displaced from the exact bridging site identified in the SEXAFS study.

In our new PhD study presented here, we find, on the basis of the R -factor values alone,

comparably acceptable bridging and hollow site models. However, if we impose reasonable constraints on the conformation of the adsorbed SO₂ molecule, only the hollow site geometry is acceptable. Lower *R*-factor values can be obtained for an unconstrained bridging model, but applying reasonable constraints to the intramolecular bondlengths and bond angle leads to unacceptably high *R*-factors. In many ways, this situation is somewhat similar to that involved in the analysis of the NIXSW data. For a small flat-lying adsorbed molecule, intramolecular scattering is relatively unimportant in PhD spectra, at least at near-normal emission geometries such as those found to give the strongest modulations in the present study. The PhD modulations are then sensitive primarily to the local adsorption site of the S and O atoms individually, and not to the juxtaposition of these atoms. NIXSW is *only* sensitive to the local sites of the constituent atoms, and has no sensitivity to their relative positions. In order to interpret these data in terms of molecular adsorption sites, one must therefore ask how S and O atoms can be arranged in the local sites given by the experimental data, in such a way as to construct an adsorbed molecule with a plausible molecular conformation. In the present case of SO₂ on Ni(111), the answer is that only adsorption in a hollow site satisfies these constraints.

In view of the evident disagreement with the conclusions of the earlier SEXAFS study, it is appropriate to consider these earlier data in more detail. One important initial remark is that, in identifying the S adsorption site from these data, Yokoyama *et al.* only considered the highest-symmetry sites, notably that the S atom occupies (exactly) either atop, bridge or hollow sites. Could their data be compatible with our preferred geometry? In SEXAFS the adsorption site is determined by measuring the amplitude of the EXAFS oscillations as a function of the direction of the polarisation vector of the incident X-rays. This amplitude is related to the effective number of nearest neighbours 'seen' by the measurement, N^* (see, e.g. [19]). By determining the intensity ratio with the polarisation vector at angles of 55° and 15° from the surface normal, $N^*(55)/N^*(15)$ to be 0.53 ± 0.05 , they effectively determined the angle of the S-Ni nearest-neighbour bond, relative to the surface normal, to be $35 \pm 4^\circ$, compatible with their expectation for the ideal bridging site of 35.2° . Clearly, some displacement from the exact bridging site could also be compatible with these data, but the off-atop geometry we favour in our hollow site model

(table 2) corresponds to a S-Ni bond angle of 19° , which differs from the measurement by significantly more than the estimated errors. We note, though, that the optimised off-bridge geometry of the recent DFT calculations yields a S-Ni bond angle of 21.5° , also apparently incompatible with the experimental SEXAFS value. Inspection of the published NEXAFS spectra of Yokohama *et al.* suggests one possible explanation for this discrepancy, namely the role of coadsorbed atomic S. As also seen in our own data (e.g. fig. 2), even with adsorption at low temperature, some fraction of the SO_2 deposited on the surface fragments, leading to coadsorbed atomic S. The NEXAFS spectra published by Yokohama *et al.* [1] seem to show that in their experiments this could account for 20% or more of the total S coverage (if the associated pre-edge feature is an edge-jump, rather than an unresolved peak), although the XPS spectrum in the same paper does suggest the amount may be significantly less. Unlike our PhD measurements, however, SEXAFS does not offer chemical-state specificity, so the measured spectra are some weighted average of the individual SEXAFS from the co-adsorbed S-containing surface species. Atomic S occupies hollow sites on Ni(111) [20] that are significantly closer to the surface than is S in SO_2 , leading to a much-increased S-Ni bond angle relative to the surface normal of $\sim 42^\circ$. As a result, the true value of the S-Ni bond angle for the SO_2 species will be smaller than the 'average' value of 35° inferred from the SEXAFS data, by an amount that depends on the relative coverage of atomic S.

Comparison of the structural parameters obtained in different studies listed in Table 2 shows that there is excellent agreement in the lateral offsets of the S and O atoms from the atop sites between the NIXSW study and the new PhD results. The offsets found for this geometry in the recent DFT study do differ somewhat; the two experimental studies yield lateral offsets from atop sites that are almost identical for the S and O atoms, whereas the DFT structure has the molecule centred further from the exact hollow site. However, the DFT study revealed a very shallow minimum in the dependence of the total energy on the exact offset, so this discrepancy is perhaps not surprising. More surprising, however, is the fact that the PhD structural solution indicates that the molecule is significantly closer to the surface (by 0.08-0.11 Å) than is found in the NIXSW and DFT studies, and indeed that the S-Ni nearest-neighbour bondlength is similarly shorter than

that found in the SEXAFS study. This result is somewhat surprising. There are certainly other examples of discrepancies of this level between experiment and DFT calculations for molecular adsorbates, and differences between PhD and NIXSW can arise due to near-surface relaxations of the substrate. However, PhD and SEXAFS obtain the nearest neighbour bondlengths on the basis of the same physical principles, and both generally give precise values; a discrepancy of 0.13 ± 0.04 Å is difficult to understand. Nevertheless, in all other respects, the PhD, NIXSW, and DFT studies of this system do provide a rather consistent picture of the local geometry, and we have identified one possible reason for the disagreement in adsorption site with the conclusions of the SEXAFS investigation.

4.2 SO₃

Based on the O 1s PhD data analysis alone, we are unable to distinguish three distinct local adsorption geometries for SO₃ on Ni(111) which differ primarily in the lateral position on the surface. Interestingly, none of these models correspond to the structure that was favoured in an earlier NIXSW study [6] of this system; a structure similar to this did yield a low overall *R*-factor value in the initial space search, but was rejected due to the high *R*-factor for the spectrum at 20° emission angle. As a further check on the appropriateness of this rejection criteria, a final set of calculations were undertaken, re-optimising all parameters for this model using the larger set of six PhD spectra. The results showed that an acceptably low *R*-factor could be achieved for this structure, but only using an anomalously large vibrational amplitude of the O atoms parallel to the surface (an rms value of 0.21 Å), yet also with strongly-correlated vibrations with the near-neighbour Ni atoms perpendicular to the surface; with more physically reasonable values of these parameters the *R*-factor falls just outside the acceptable range. We may therefore ask whether any one, or more, of the three preferred structures identified in the present PhD study can also be reconciled with the NIXSW experimental data.

In order to achieve this reconciliation, some explanation of the NIXSW technique is required; fuller details may be found elsewhere [6, 21]. NIXSW provides information on the location of absorbed atoms (in this case S and O) relative to different sets of bulk crystallographic atomic scatterer planes. For each set of such planes investigated, one obtains two parameters, the coherent position and the coherent fraction. If all atoms of a particular type have the same location relative to these planes, the coherent fraction is effectively an order parameter, expected in this case to be close to unity (between ~ 0.8 and 1.0), and the coherent position provides the spacing of the absorber atoms relative to the bulk crystallographic scatterer planes. Using the (111) scatterer planes parallel to the Ni(111) surface, the NIXSW results are consistent with no more than a narrow distribution of atomic heights above the surface, and give the S-Ni and O-Ni interlayer spacings shown in Table 3, which are generally in reasonable agreement with all three of the models derived from the PhD data. Note that using only O 1s PhD spectra, the S atom only influences the data through intramolecular scattering, so the precision of the S height above the surface obtained in our PhD study is poor; because the S atoms are higher above the surface than the O emitter atoms, this effect is not negligible (as in the case of SO_2), but it is not large. Notice that the O-Ni interlayer spacing obtained in NIXSW represents some weighted average of the two different values in the geometries considered in this study. In addition to this information on interlayer spacings, the NIXSW measurements relative to the $(\bar{1}11)$ scatterer planes (inclined some 70° relative to the surface) provide a measure of the lateral position of the S and O atoms on the surface, through triangulation of the coherent positions in the two measurement geometries. For low symmetry sites, and multiple sites, the data interpretation is somewhat less routine. However, a key result is that, for a given height of an adsorbed atom above the surface, the $(\bar{1}11)$ coherent position can take only one of three possible values which correspond to one of the three fully-symmetric adsorption sites, namely the fcc hollow, the hcp hollow and the atop site. Indeed, if the sites equivalently-located relative to the fcc and hcp sites are occupied with equal probability, as appears to be the case for both SO_x species on Ni(111), only two possible values of the $(\bar{1}11)$ coherent position are possible. If the absorber atom is exactly at one of the high-symmetry sites the coherent fraction is

high. If it is displaced from a high-symmetry site, the coherent fraction falls but the coherent position remains fixed until the absorber becomes closer to another high-symmetry site, at which position the coherent position value switches to the new allowed value, and the coherent fraction passes through zero.

For SO_3 on $\text{Ni}(111)$, the $(\bar{1}11)$ and (111) coherent position values for both S and O correspond to atop site triangulation, but in both cases the $(\bar{1}11)$ coherent fractions are low; for the single S atom this indicates that the site must be significantly displaced from atop. In the case of the O atoms, occupying at least two inequivalent sites, some reduction could arise from an appropriate mixture of off-atop and off-hollow sites. The fact that the NIXSW data show that the S atom must be closer to an atop site than a hollow site is clearly not compatible with either model 'a' or model 'c'. Notice, too, that model 'a' has all three O atoms very close to atop sites, incompatible with the low $(\bar{1}11)$ coherent fraction for this species. Model 'b', on the other hand, does potentially have the right structural ingredients to match the NIXSW data. The S atom is in an off-atop site, while the O atoms are in a mixture of off-atop and off-hollow sites. Fig. 9 shows a more quantitative evaluation of these arguments in the form of coherent fraction contour maps of all possible sites on the $\text{Ni}(111)$ surface, assuming equivalence of the two hollow sites in occupation probability. The panel on the left reproduces that used in the original NIXSW structure determination [6]. The dark ring around the Ni atom corresponds to the range of off-atop locations that match the measured S $(\bar{1}11)$ coherent fraction (and the measured coherent position as off-atop). According to the NIXSW data, the S atom must lie somewhere within the dark shading of this ring. The O atoms occupy two inequivalent sites. The atom on the right is rather close to atop (with a high component coherent fraction); the two equivalently-located O atoms on the left occupy off-hollow sites, but with low individual coherent fractions. As explained in detail in the original paper, this combination leads to coherent position and fraction values that agree well with the experimental measurements. This model does not, however, correspond to one of the preferred PhD solutions. However, on the right is shown model 'b' of the PhD analysis, similarly superimposed on the $(\bar{1}11)$ coherent fraction contour map. Relative to the left-

hand panel, in the new model the molecule is displaced to the left so that the S atom now sits on the dark ring of preferred sites relative to the adjacent Ni atom. The right-hand O atom has now shifted from the right to the left of the ideal atop site, but lies on essentially the same off-atop contour line, while the two left-hand O atoms are also on off-hollow contour lines of the same value as the original model. Clearly, therefore model 'b' is compatible with both the PhD and NIXSW data.

5. Conclusions

The PhD technique has been applied to the problem of determining, in a fully quantitative fashion, the local adsorption structure of the SO₂ and SO₃ species on Ni(111). For SO₂, useful PhD spectra were obtained from both the O 1s and S 2p emission, allowing a largely independent determination of the off-atop local adsorption sites of the constituent atoms. These can be related to two alternative models of the local molecular adsorption geometry, one with the molecule in hollow sites, the other in a bridging site. On the basis of the PhD *R*-factors alone, these two models cannot be distinguished, but by applying reasonable constraints on the molecular conformation, most notably on the S-O bondlength (for which experimental information exists from SEXAFS measurements), we find that only the hollow site geometry is acceptable. This conclusion is in agreement with an earlier NIXSW study, and consistent with DFT calculations, but inconsistent with the conclusions of an earlier SEXAFS study. We suggest, however, that this inconsistency may be a result of the lack of chemical-state specificity in SEXAFS which means that other coadsorbed S species (notably atomic S) will influence the results of the SEXAFS measurement.

For adsorbed SO₃, the S 2p PhD spectra showed modulations that were too weak to provide useful quantitative information on the structure, possibly a consequence of the fact that the S atom appears to not be directly involved in the bonding to the surface, and is significantly more distant than the O atoms from the strongly-scattering Ni atoms in the surface. Using O 1s PhD spectra alone leads to three possible local adsorption geometries that give comparably good agreement with experiment. However, only one of these three

structures is shown to be compatible with previously-published NIXSW measurements. Interestingly, the one mutually acceptable solution differs from that originally proposed in the NIXSW study in the location of the molecule, although the local positions of the constituent S and O atoms to the Ni surface are essentially the same.

Obtaining quantitative and unique surface structures for molecular adsorbates adopting low-symmetry geometries is a challenging problem in surface science, and the PhD alone is not always able to fully solve this problem. In combination with additional information from other methods, however, this challenge has been met in the systems studied here.

Acknowledgements

The authors acknowledge the financial support of the Physical Sciences and Engineering Research Council (UK) and the award of beamtime at the BESSY II facility.

Table 1

Summary of the different structural solutions corresponding to minima in the R -factor for the S 2p and O 1s PhD data and simulations obtained in different optimisations. For each structure two values of the R -factor are given, the initial value obtained in the structural optimisation and, in parentheses, the value obtained for this structure from more fully-converged calculations using a larger number of scattering pathways. In the case of the hollow site geometry only the results of a free optimisation of all parameters is shown. For the bridge site geometry, the table includes the results of further optimisations in which either the S-O bondlength or the O-S-O bond angle (values marked *) were constrained to pre-selected values broadly consistent with expectations based on the gas-phase geometry or previous experimental studies.

structural model	S-O bondlength	O-S-O bond angle	O off-atop displacement	R -factor
hollow	1.50 Å	111°	0.66 Å	0.19 (0.23)
bridge	1.48 Å *	140°	0.78 Å	0.20 (0.22)

bridge	1.52 Å *	140°	0.74 Å	0.20 (0.22)
bridge	1.52 Å	110° *	0.93 Å	0.33 (0.38)
bridge	1.76 Å	124°	0.62 Å	0.16 (0.19)

Table 2

Structural parameter values obtained for SO₂ adsorption on Ni(111) in this study and in other published experimental and theoretical investigations. In the present study the parameters for occupation of the two different (fcc and hcp) hollow sites are prefixed by 'f' and 'h', respectively, when these values differ. In the slab DFT calculations [9] two values are entered in some places due to inequivalence of the two different O atoms within the molecule. The value marked * corresponds to a parameter that was fixed in the NIXSW data analysis.

structural model	hollow	hollow	hollow	hollow	bridge	bridge	bridge
d_{S-O} (Å)	1.50±0.04	1.51	1.48*	1.50 ±0.02	1.54, 1.53	1.67	1.48 ±0.03
O-S-O angle (°)	111±5	108	110	110±5		102	
d_{Ni-S} (Å)	f 2.05±0.03 h 2.04±0.03	2.16	2.12	2.5±0.1	2.16	2.30	2.16 ±0.03
d_{Ni-O} (Å)	f 1.97±0.02 h 1.94±0.02	2.05, 2.04	2.05	2.0±0.1	2.09, 2.18	2.02	
z_{Ni-S} (Å)	f 1.94±0.03 h 1.93±0.03	2.07	2.02 ±0.05		2.01	2.15	
z_{Ni-O} (Å)	f 1.86±0.02 h 1.83±0.02	2.00	1.94 ±0.05		1.94	1.76	
xy_{Ni-S} (Å)	0.65±0.08	0.85	0.65 ±0.05		0.63		1.25
xy_{Ni-O} (Å)	0.66±0.07	0.45, 0.42	0.65 ±0.05		0.77, 1.00		
method/ [reference]	PhD [this study]	DFT [9]	NIXSW [6]	NEXAFS [7]	DFT [9]	DFT [8]	SEXAFS [1, 2]

Table 3

Structural parameter values obtained for the three alternative models for SO₃ adsorption on Ni(111) found in this study, together with the results of the other published experimental (NIXSW) investigation.

structural model	'a'	'b'	'c'	NIXSW [6]
$z_{\text{Ni-O}}$ (Å)	2.00, 1.85, 1.85±0.03	1.92, 1.78, 1.78±0.03	1.86, 1.66, 1.66±0.04	1.82±0.05 'average'
$z_{\text{Ni-S}}$ (Å)	2.67±0.18	2.56±0.18	2.54±0.18	2.69±0.05
$xy_{\text{Ni-O}}$ (Å)	0.44, 0.42, 0.42±0.16	0.20, 1.13, 1.13±0.06	1.28, 1.27, 1.27±0.03	see text
$d_{\text{Ni-O}}$ (Å)	2.05, 1.90, 1.90±0.03	1.93, 2.11, 2.11±0.03	2.26, 2.09, 2.09±0.05	
O-S-O angle (°)	101, 96, 101±7	101, 94, 101±7	92, 98, 92±8	110±5
molecular axis tilt (°)	4.0±1.5	3.9±3.3	6.4±1.6	

Figure Captions

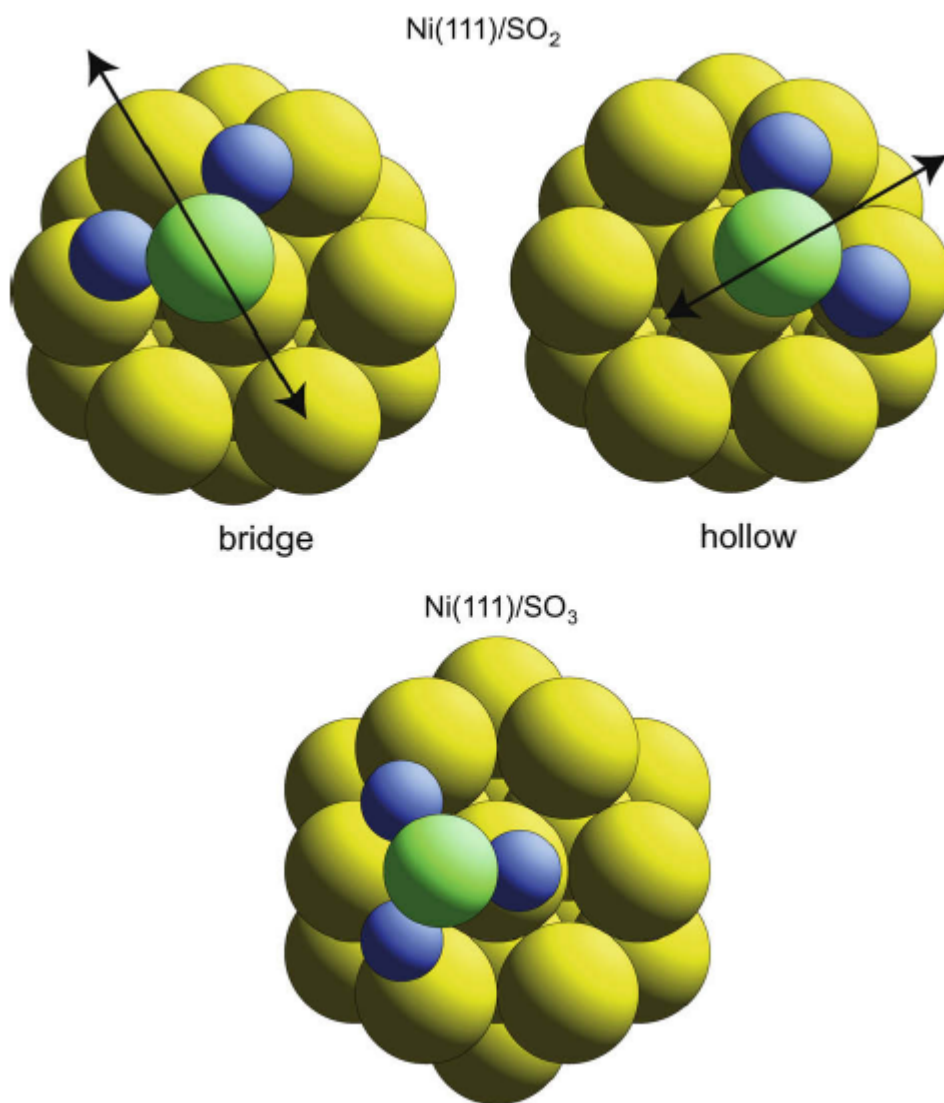


Fig. 1 Schematic plan views of the bridge and hollow SO_2 adsorption geometries on $\text{Ni}(111)$, and of the NIXSW-optimised adsorption geometry for SO_3 . For SO_2 the actual geometries shown here are those found in a recent DFT investigation [9]. Note that the original proposal for the bridge site model (based on SEXAFS experiments [1]) had the S atom (rather than the whole molecule) exactly in the bridging site. The arrows indicate the directions in which the molecules were displaced in the 'space-searching' PhD calculations.

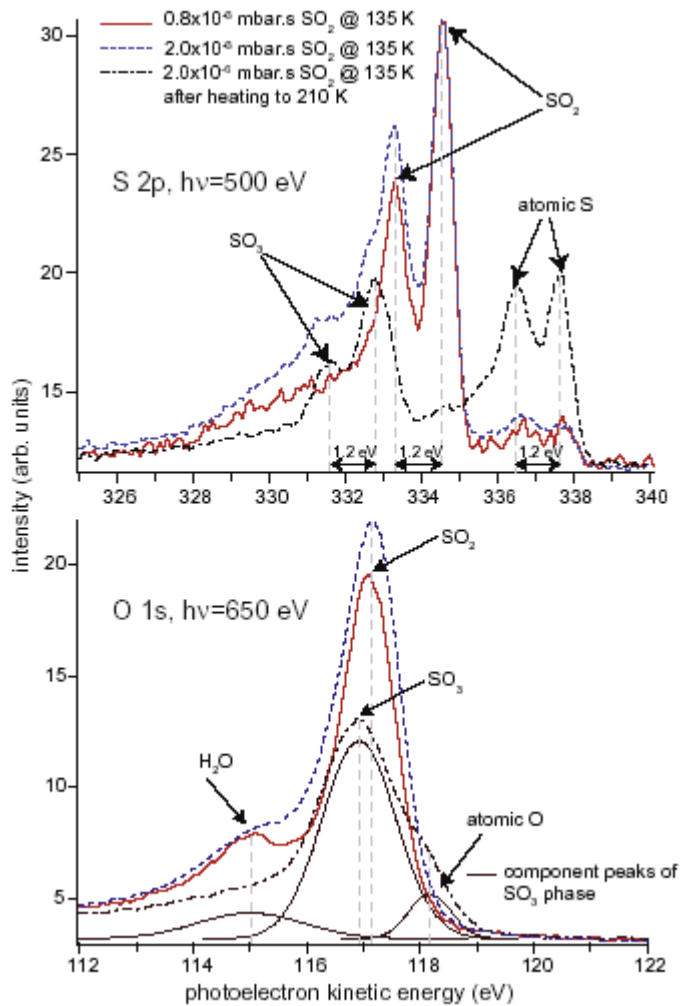


Fig. 2 S 2p and O 1s XP spectra from the Ni(111) surface after SO_2 dosing and subsequent heating to 210 K

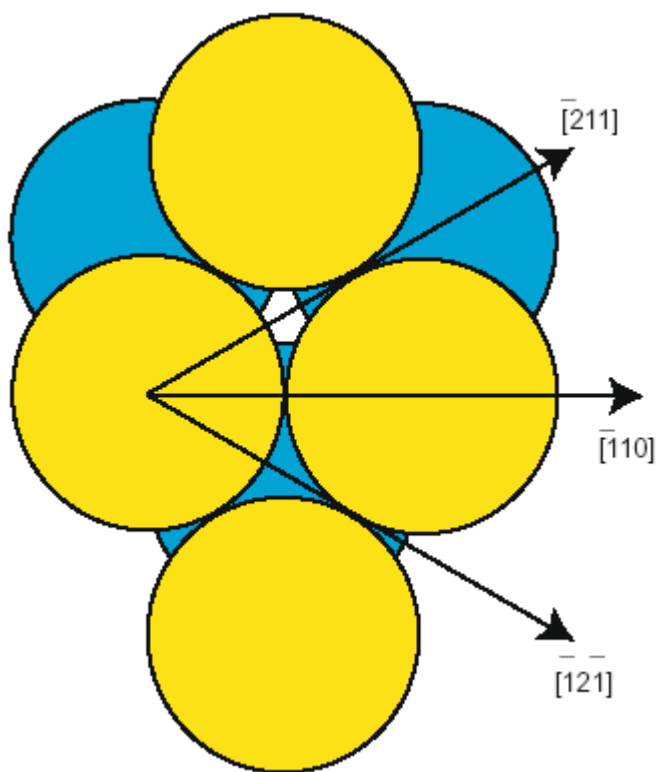


Fig. 3 Plan view of the Ni(111) surface showing the definition of azimuthal directions in which PhD spectra were recorded

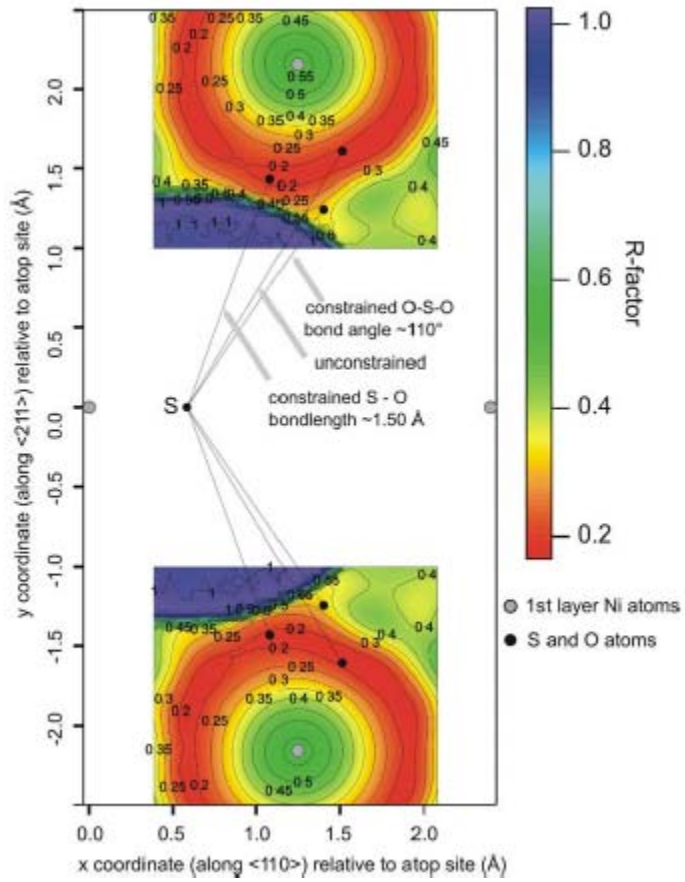


Fig. 4 Partial contour maps of the PhD R -factor values for different positions of the O atoms on the Ni(111) surface obtained in calculations based on the bridging-site model of SO_2 adsorption. The location of the outermost layer Ni and the S atom are also shown.

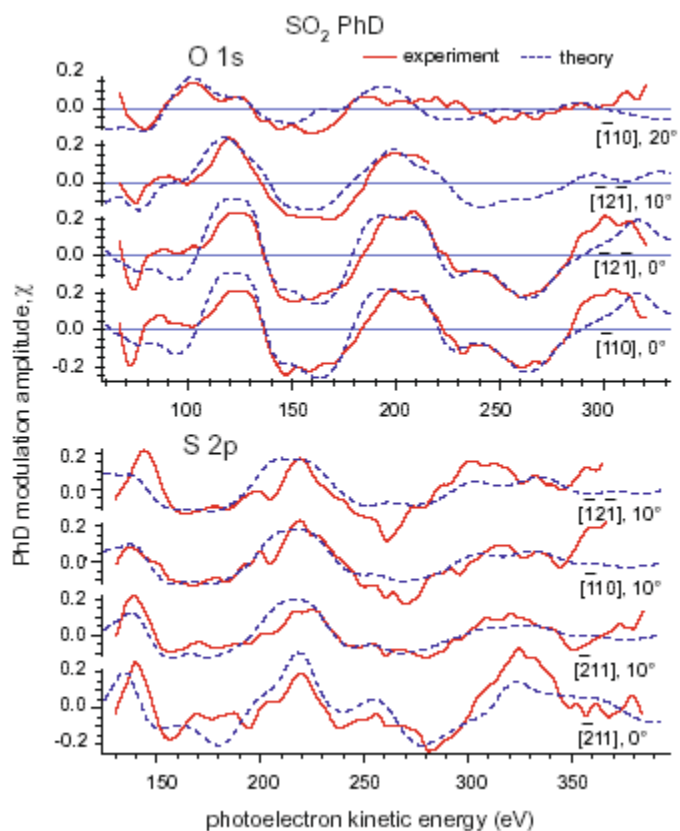


Fig. 5 Comparison of experimental O 1s and S 2p PhD modulation spectra from SO₂ on Ni(111) with the results of theoretical simulations for the best-fit hollow-site structural model. The structural parameter values are listed in Table 2.

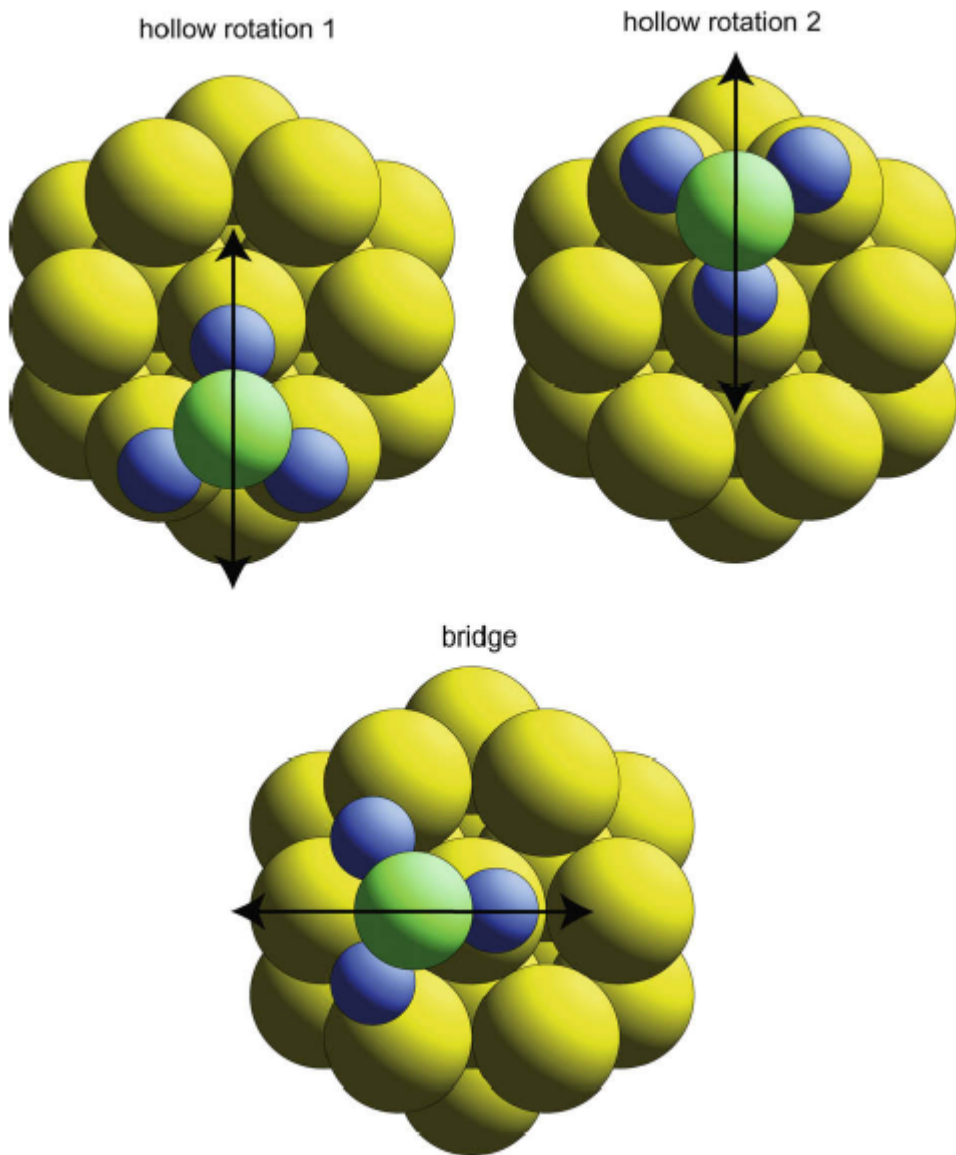


Fig. 6 Starting models used in the 'space-searching' calculations of possible SO₃ adsorption geometries on Ni(111). The arrows indicate the directions in which the molecules were displaced in the 'space-searching' PhD calculations.

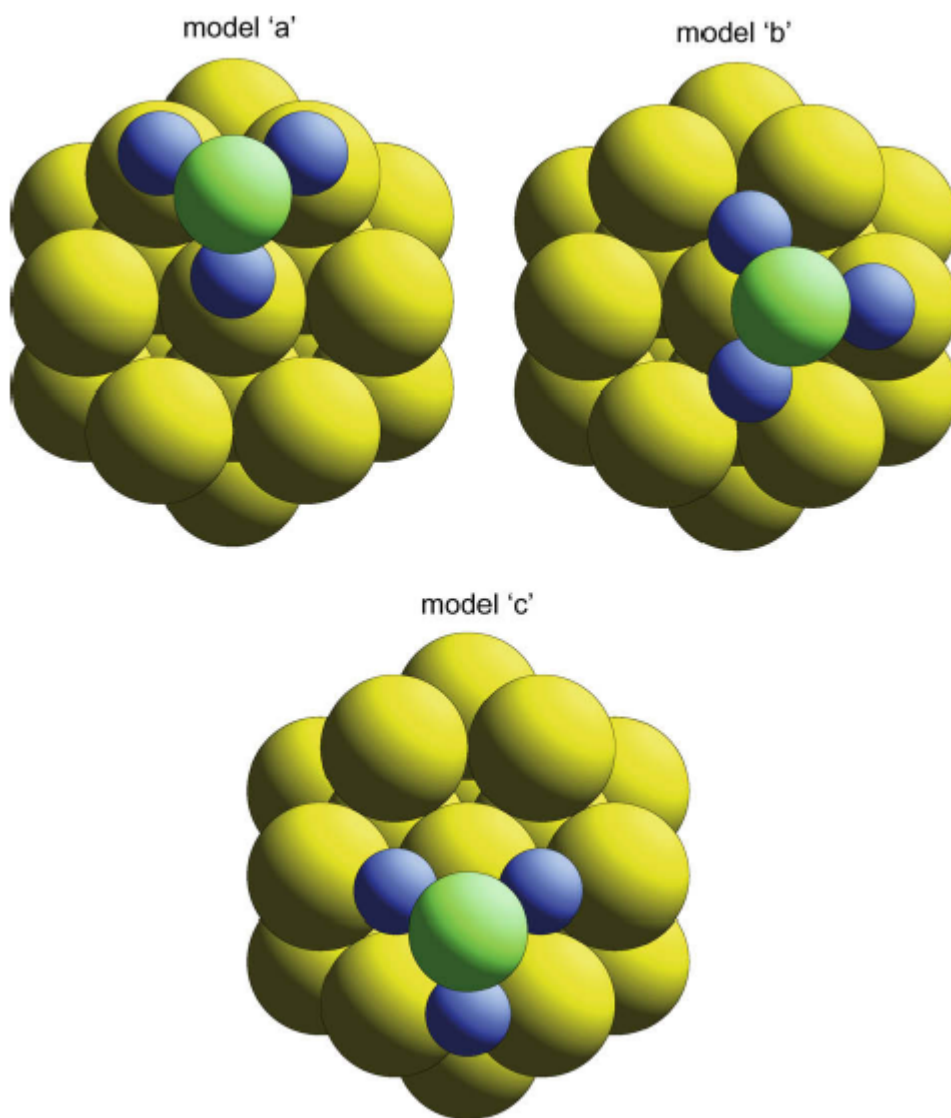


Fig. 7 Schematic plan views of the three best-fit structural models for SO_3 on Ni(111) on the basis of the O 1s PhD data analysis. The associated structural parameter values are listed in Table 3.

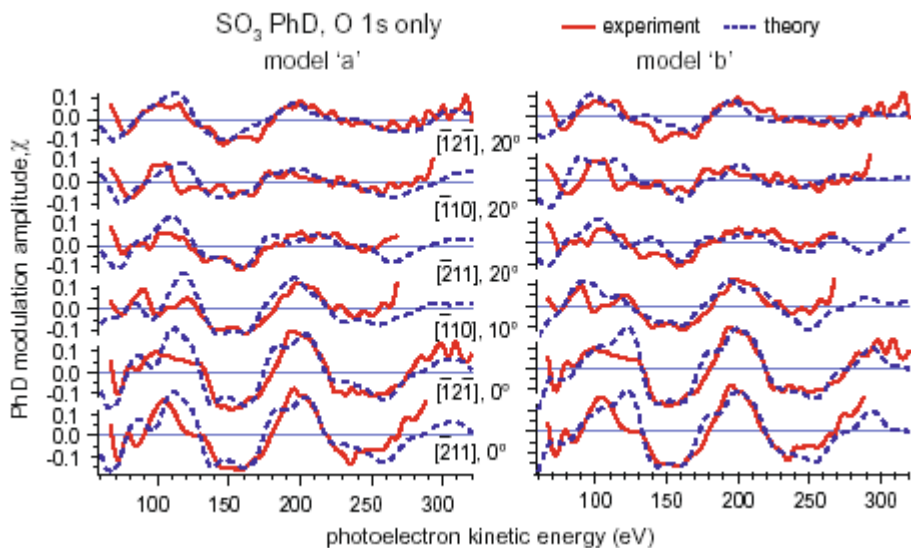


Fig. 8 Comparison of experimental O 1s PhD modulation spectra from SO₃ on Ni(111) with the results of theoretical simulations for the best-fit structural models 'a' and 'b' (see fig. 7 and Table 3)

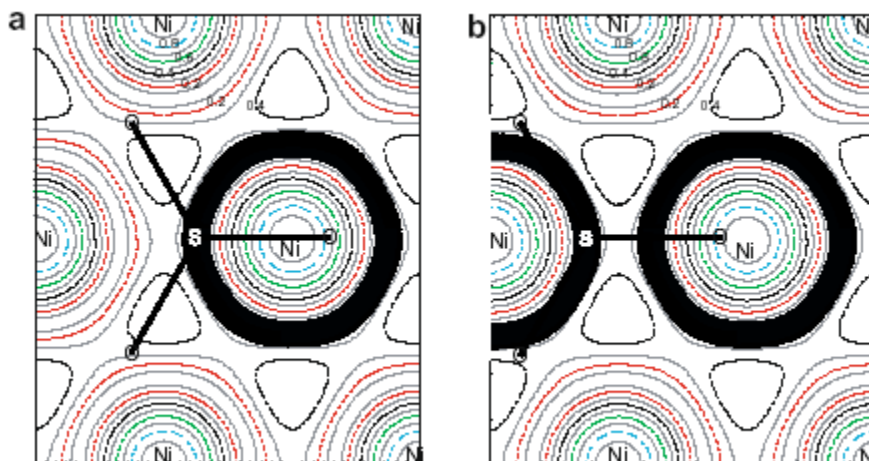


Fig. 9 NIXSW (111) coherent fraction contour maps of the Ni(111) surface with two alternative local adsorption geometries superimposed, as described more fully in the text. (a) shows the model based on the original interpretation of the NIXSW data [6]. (b) shows the model proposed here based on the PhD data which corresponds to model 'b' of fig. 7 and Table 3.

References

- 1 T. Yokoyama, S. Terada, S. Yagi, A. Imanishi, S. Takenaka, Y. Kitajima, T. Ohta, Surf. Sci. 324 (1995) 25.
- 2 T. Yokoyama, A. Imanishi, S. Terada, H. Namba, Y. Kitajima, T. Ohta, Surf. Sci. 334 (1995) 88.
- 3 S. Terada, A. Imanishi, T. Yokoyama, S. Takenaka, Y. Kitajima, T. Ohta, Surf. Sci. 336 (1995) 55.
- 4 L. Wilde, M. Polcik, J. Haase, B. Brena, D. Cocco, G. Comelli, G. Paolucci, Surf. Sci. 405 (1998) 215.
- 5 G. J. Jackson, J. Lüdecke, S. M. Driver, D. P. Woodruff, R. G. Jones, A. Chan, B. C. C. Cowie, Surf. Sci. 389 (1997) 223.
- 6 G. J. Jackson, D. P. Woodruff, A. S. Y. Chan, R. G. Jones, B. C. C. Cowie, Surf. Sci. 577 (2005) 31.
- 7 S. Cao, J.-C. Tang, P. Zhu, L. Wang, J. Phys.: Condens. Matter 13 (2001) 5865.
- 8 Y. Sakai, M. Koyanagi, K. Mogi, E. Moyoshi, Surf. Sci. 513 (2002) 272.
- 9 M.J. Harrison, D.P. Woodruff, J. Robinson, Surf. Sci. 600 (2006) 1827.
- 10 K.J.S. Sawhney, F. Senf, M. Scheer, F. Schäfers, J. Bahrtdt, A. Gaupp and W. Gudat, Nucl. Instrum. Methods A 390 (1997) 395.
- 11 D.P. Woodruff and A.M. Bradshaw Rep. Prog. Phys. 57 (1994) 1029.
- 12 D. P. Woodruff, Surf. Sci. Rep. 62 (2007) 1.
- 13 V. Fritzsche, Surf. Sci. 213 (1989) 648.
- 14 V. Fritzsche, Surf. Sci. 265 (1992) 187.
- 15 R. Dippel, K.U. Weiss, K.M. Schindler, P. Gardner, V. Fritzsche, A.M. Bradshaw, M.C. Asensio, X.-M. Hu, D.P. Woodruff and A.R. González-Elipe, Chem. Phys. Lett. 199 (1992) 625.
- 16 J. B. Pendry, J. Phys. C 13 (1980) 937.
- 17 N. A. Booth, R. Davis, R. Toomes, D. P. Woodruff, C. Hirschmugl, K.-M. Schindler, O. Schaff, V. Fernandez, A. Theobald, Ph. Hofmann, R. Lindsay, T. Giessel, P. Baumgärtel and A. M. Bradshaw, Surf. Sci. 387 (1997) 152.
- 18 A. H. Clark, B. Beagley, Trans. Farad. Soc 67 (1971) 2216.

-
- 19 D.P. Woodruff, T.A. Delchar, *Modern Techniques of Surface Science – Second Edition*, CUP, Cambridge, 1994, p168.
- 20 J. Lüdecke, A.R.H.F. Ettema, S.M. Driver, G. Scragg, M. Kerkar, D.P. Woodruff, B.C.C. Cowie, R.G. Jones, S. Bastow *Surf. Sci.* 366 (1996) 260, and references therein.
- 21 D.P. Woodruff, *Rep. Prog. Phys.* 68 (2005) 743.